On the Electronic and Structural Properties of Tri-Niobium Oxide Clusters $Nb_3O_n^-$ ($n = 3-8$): Photoelectron Spectroscopy and Density Functional Calculations

Wen-Jie Chen,[†,‡] Hua-Jin Zhai,[§] Yong-Fan Zhang,[†,‡] Xin Huang,*[,†,‡] and Lai-Sheng Wang*[,§]

Department of Chemistry, Fuzhou University, Fuzhou, Fujian 350108, P. R. China, State Key Laboratory of Structural Chemistry, Fuzhou, Fujian 350002, P. R. China, and Department of Chemistry, Brown University, Providence, Rhode Island 02912

Received: March 17, 2010; Revised Manuscript Received: April 20, 2010

The electronic and structural properties of a series of triniobium oxide clusters, $Nb_3O_n^-$ and Nb_3O_n ($n = 3-8$), are investigated using photoelectron spectroscopy (PES) and density functional theory (DFT) calculations. PES spectra are obtained for $Nb_3O_n^-$ ($n = 3-8$) at various photon energies and are used to compare with the DFT calculations. A trend of sequential oxidation is observed as a function of O content until $Nb_3O_8^-$, reaching the highest oxidation state of Nb. DFT calculations are performed to search for the lowest energy structures for both the anionic and neutral clusters. For $Nb_3O_3^-$, the three O atoms are shown to prefer the bridging sites of a triangular Nb_3, leading to two nearly degenerate cyclic structures of C_s symmetry. The next three O atoms from $n = 4-6$ each occupy a terminal site directly bonded to Nb, resulting in a symmetric $Nb_3O_6^-$ with C_{3v} symmetry and a low-lying isomer of C_s symmetry. The seventh O atom is bonded to two Nb atoms forming a double bridge, whereas the eighth O atom is bonded to a terminal site so that in $Nb_3O_8^-$ each Nb atom reaches its maximum oxidation state of +5. The structures and electronic states for the triniobium oxide clusters are significantly different from the corresponding tritantalum oxide clusters, in particular, for $Nb_3O_3^-$, $Nb_3O_5^-$, and $Nb_3O_7^-$. Molecular orbital analyses are performed to elucidate the chemical bonding and the electronic and structural evolution in these triniobium oxide clusters.

1. Introduction

There is increasing interest in niobium-containing compounds and materials, which are important and widely used in catalysis.[1−6] Niobium oxides are particularly important because of their structural diversity and applications as a catalyst support.[2] There is evidence that niobium oxides are good catalytic promoters.[3] Understanding the catalytic effects of niobium oxides at the molecular level can help design better catalysts. Gas-phase cluster studies can provide valuable structural models and mechanistic information for real world catalysis.[7] Following our previous work on the metal-rich triniobium oxide clusters $Nb_3O_n^-$ ($n = 0-2$),[8] we study in the current work systematically the O-rich triniobium oxide clusters, $Nb_3O_n^-$ and Nb_3O_n ($n = 3-8$), reaching the highest oxidation state of Nb in $Nb_3O_8^-$. We combine photoelectron spectroscopy (PES) and density-functional theory (DFT) calculations to understand their chemical bonding and electronic and structural evolution as a function of composition.

Small niobium clusters and niobium oxide clusters have been studied in a number of previous experimental[9−24] and theoretical works.[13,18,22,24−35] Collision-induced dissociation (CID) suggested that $Nb_3O_7^+$ might be the core for larger clusters $Nb_3O_{8-9}^+$.[15] Photodissociation of $M_mO_n^+$ (M = V, Nb, Ta) revealed that MO_2^+, $M_3O_7^+$, $M_5O_{12}^+$, and $M_7O_{17}^+$ are the most stable cation stoichiometries.[19] Using single photon ionization at 26.5 eV for M_mO_n (M = V, Nb, Ta), Dong et al. identified the general form $(MO_2)_{0,1}(M_2O_5)_n$ ($n = 1-4$) as the most abundant neutral clusters.[20] Sambrano et al. investigated the geometric, thermodynamic, and electronic properties of $Nb_mO_n^{0/+}$ ($m = 1-3$; $n = 2-5$, 7, 8) clusters using DFT calculations and suggested that the $Nb_3O_n^{0/+}$ ($n = 7$, 8) clusters possess chain structures.[29]

For anionic niobium oxide clusters, Sigsworth et al. reported gas-phase reactions of the negatively charged oxides of tantalum, niobium, vanadium, and tungsten with O_2, HCl, and H_2O.[21] Jackson et al. studied gas-phase reactions of NbO_3^- and $Nb_mO_n^-$ clusters with methanol and ethanol and proposed three possible structures for $Nb_3O_8^-$.[23] However, precise knowledge of the structures and chemical bonding of the niobium oxide clusters is a prerequisite to understanding their chemical reactivity. The current work continues our interest in developing cluster models[8,36,37] for early transition-metal oxide catalysts and in elucidating the structures and chemical bonding in both stoichiometric and nonstochiometric niobium oxide clusters.[38,39] We have previously studied a metal-rich $Ta_3O_3^-$ cluster and found that it possesses a highly symmetric D_{3h} structure with significant metal−metal bonding and δ aromaticity.[38] We further investigated the structures and chemical bonding systematically of the whole series of trinuclear tantalum oxide clusters, $Ta_3O_n^-$ ($n = 0-8$).[36] However, our preliminary study of the $Nb_3O_n^-$ ($n = 0-2$) clusters[8] found that $Nb_3O_2^-$ is unusual, in which the second O atom is shown to prefer a terminal site, quite different from that in the $Ta_3O_2^-$ cluster. Because we expected that the Nb and Ta oxide systems should be similar, a question arises: are there other cases where Nb and Ta clusters with the same metal−oxygen compositions have different structures?

The current study focuses on the larger trinuclear niobium oxide clusters, $Nb_3O_n^-$ ($n = 3-8$). Well-resolved PES data have been measured at different photon energies. DFT calculations are performed to optimize the structures of both the anion and neutral clusters. PES spectra are simulated and compared with

* Corresponding author. E-mail: xhuang@fzu.edu.cn; Lai-Sheng_Wang@brown.edu.
† Fuzhou University.
‡ State Key Laboratory of Structural Chemistry.
§ Brown University.

10.1021/jp102439v © 2010 American Chemical Society
Published on Web 04/29/2010

the experimental data to verify the obtained global minimum structures and low-lying isomers. The evolution of the electronic structure and chemical bonding as a function of composition is analyzed. We are particularly interested in comparing the Nb and Ta systems. We found indeed that $Nb_3O_3^-$ is significantly different from the δ-aromatic $Ta_3O_3^-$ cluster. We further found that the potential energy surfaces of the triniobium oxide clusters are fairly flat, resulting in multiple isomers with close energies, specifically for the $Nb_3O_3^-$, $Nb_3O_5^-$, and $Nb_3O_7^-$ clusters, which are borne out in the experimental data.

2. Experimental and Computational Methods

2.1. Photoelectron Spectroscopy. The experiment was carried out using a magnetic-bottle PES apparatus equipped with a laser vaporization cluster source, details of which have been described elsewhere.[40] In brief, the $Nb_3O_n^-$ clusters were produced by laser vaporization of a niobium disk target in the presence of a pure He carrier gas (for $n = 3$ and 4) or a He carrier gas seeded with 0.01% O_2 (for $n = 5-8$). The trace amount of oxygen in the He carrier gas or residual oxygen on the target surface was sufficient to produce abundant $Nb_3O_3^-$ and $Nb_3O_4^-$ clusters for the current study. The cluster anions were analyzed using a time-of-flight mass spectrometer, and the $Nb_3O_n^-$ clusters of interest were each mass-selected and decelerated before being photodetached. Four detachment photon energies were used in the present work: 532 (2.331 eV), 355 (3.496 eV), 266 (4.661 eV), and 193 nm (6.424 eV). Effort was made to choose colder clusters (i.e., those with long resident times in the nozzle) for photodetachment, which was shown previously to be important for obtaining high quality PES data.[41] Photoelectrons were collected at nearly 100% efficiency by the magnetic-bottle and analyzed in a 3.5 m long electron flight tube. The PES spectra were calibrated using the known spectra of Au^- and Rh^-, and the energy resolution of the apparatus was $\Delta E/E \approx 2.5\%$, that is, ~25 meV for 1 eV electrons.

2.2. Density Functional Calculations. Theoretical calculations were performed at the DFT level using the B3LYP hybrid functional.[42−44] A number of structural candidates including different spin states and initial structures were evaluated, and the search for the global minima was performed using analytical gradients with the Stuttgart relativistic small core potential and the valence basis sets[45,46] augmented with two *f*-type and one *g*-type polarization functions [$\zeta(f) = 0.261, 0.970$; $\zeta(g) = 0.536$] for Nb, as recommended by Martin and Sundermann[47] and the aug-cc-pVTZ basis set for oxygen.[48,49] Scalar relativistic effects, that is, the mass velocity and Darwin effects, were taken into account via the quasi-relativistic pseudopotentials. Vibrational frequency calculations were performed at the same level of theory to verify the nature of the stationary points. A selected set of anionic optimized structures (within ~0.40 eV) were tested with several exchange-correlation functionals for accuracy and consistency. The calculated results using the B3LYP and BP86[42,50] functionals are presented as Supporting Information (Table S7).

Vertical electron detachment energies (VDEs) were calculated using the generalized Koopmans' theorem by adding a correction term to the eigenvalues of the anion.[51] The correction term was estimated by $\delta E = E_1 - E_2 - \varepsilon_{HOMO}$, where E_1 and E_2 are the total energies of the anion and neutral, respectively, in their ground states at the anion equilibrium geometry, and ε_{HOMO} corresponds to the eigenvalue of the highest occupied molecular orbital (HOMO) of the anion. PES spectra were simulated by fitting the distribution of calculated VDEs with unit-area Gaussian functions of 0.1 eV width. The methods have been used in a number of previous studies and have been shown to yield VDEs in good agreement with PES data.[8,36−39] All calculations were performed with the Gaussian 03 software package.[52] Three-dimensional contours of the molecular orbitals were visualized using the VMD software.[53]

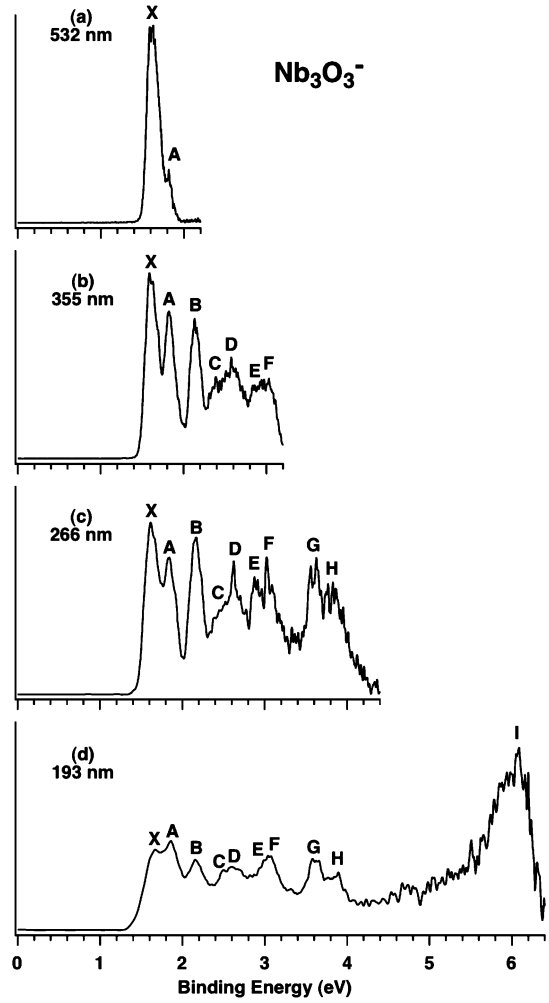

Figure 1. Photoelectron spectra of $Nb_3O_3^-$ at (a) 532 (2.331 eV), (b) 355 (3.496 eV), (c) 266 (4.661 eV), and (d) 193 nm (6.424 eV).

3. Experimental Results

The photoelectron spectra of $Nb_3O_n^-$ ($n = 3-8$) at various photon energies are shown in Figures 1−6, respectively. The observed electronic transitions are labeled with letters, and the measured adiabatic detachment energies (ADEs) and VDEs are given in Table 1 for all species.

3.1. $Nb_3O_3^-$. The 532 nm spectrum of $Nb_3O_3^-$ (Figure 1a) reveals the ground state X (VDE: 1.62 ± 0.02 eV) and the first excited state A (VDE: 1.84 eV). Because no vibrational structures are resolved for band X, the ground-state ADE is evaluated by drawing a straight line along the leading edge of band X and then adding the instrumental resolution to the intersection with the binding energy axis. Although this is an approximate procedure, we are able to obtain a consistent ADE from the well-defined spectral onsets of band X at different photon energies. The ADE thus evaluated for $Nb_3O_3^-$ is 1.54 ± 0.02 eV, which represents the electron affinity of neutral Nb_3O_3. The 355 and 266 nm spectra (Figure 1b,c) further show congested electronic transitions, among which seven bands are labeled (B: 2.15 eV; C: 2.45 eV; D: 2.60 eV; E: 2.90 eV; F:

TABLE 1: Experimental Adiabatic (ADE) and Vertical (VDE) Detachment Energies of $Nb_3O_n^-$ ($n = 3-8$) and Comparison with the Calculated VDEs from the Lowest-Energy Anion Structures at the B3LYP Level of Theory

	ADE (exptl)[a,b,c]	VDE (exptl)[a,b]	anion state	VDE (theor)[a]
$Nb_3O_3^-$	1.54 (2)	1.62 (2)	C_s (^{3}A′)	1.48
$Nb_3O_4^-$	2.15 (3)	2.26 (3)	C_s (^{1}A′)	2.07
$Nb_3O_5^-$	1.87 (3)	2.09 (5)	C_2 (^{3}A)	2.01[d]
			C_s (^{5}A″)	2.57
$Nb_3O_6^-$	3.15 (5)	3.38 (3)	C_s (^{1}A′)	3.29[d]
	∼2.7 (X′)[e]	2.84 (5) (X′)[e]	C_{3v} (^{3}A$_1$)	3.06
$Nb_3O_7^-$	3.30 (5)	3.66 (4)	C_1 (^{1}A)	3.44[d]
	∼2.5 (X′)[e]	∼2.7 (X′)[e]	C_{2v} (^{3}A$_2$)	2.93
$Nb_3O_8^-$	5.65 (5)	5.97 (4)	C_{2v} (^{1}A$_1$)	5.90

[a] All energies are in electronvolts. [b] Numbers in the parentheses represent experimental uncertainties in the last digit. [c] Electron affinity of the neutral species. [d] Second lowest among all calculated structures at the B3LYP level. [e] Minor isomer.

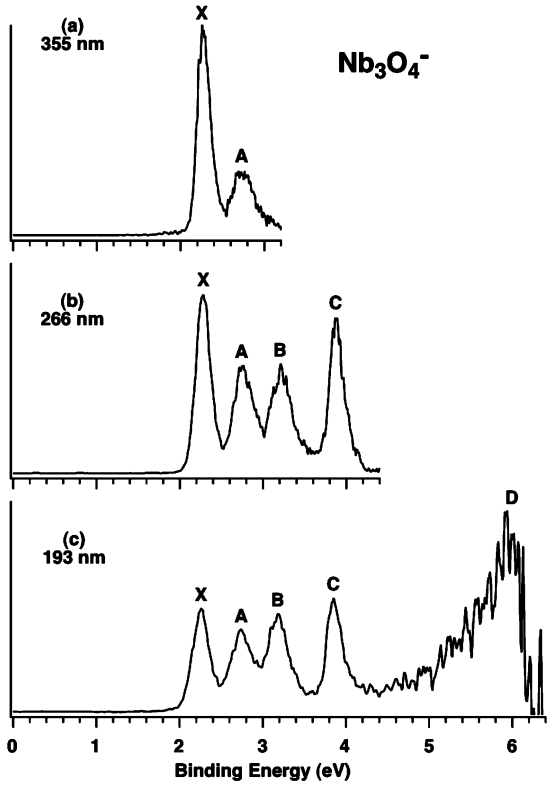

Figure 2. Photoelectron spectra of $Nb_3O_4^-$ at (a) 355, (b) 266, and (c) 193 nm.

3.03 eV; G: 3.61 eV; H: 3.85 eV). The pairs of bands C/D, E/F, and G/H are close in energy and overlapped with each other. The 193 nm spectrum (Figure 1d) reveals an intense and broad feature I at much higher binding energies (centered at ∼6.0 eV). No prominent transitions are observed in the 4.0 to 5.5 eV binding energy regime.

3.2. $Nb_3O_4^-$. The PES spectra of $Nb_3O_4^-$ (Figure 2) appear to be significantly simplified relative to those of $Nb_3O_3^-$ (Figure 1). Four well-separated bands with similar band widths are observed in the low binding energy range: X (VDE: 2.26 eV), A (2.74 eV), B (3.21 eV), and C (3.87 eV). The electron affinity of Nb_3O_4 is evaluated to be 2.15 ± 0.03 eV from the onset of band X. At the high binding energy side, a broad band D (centered at ∼5.9 eV) is observed, as shown in the 193 nm spectrum (Figure 2c). Again, no prominent transitions exist in the binding energy range of 4.0−5.5 eV, similar to those in $Nb_3O_3^-$.

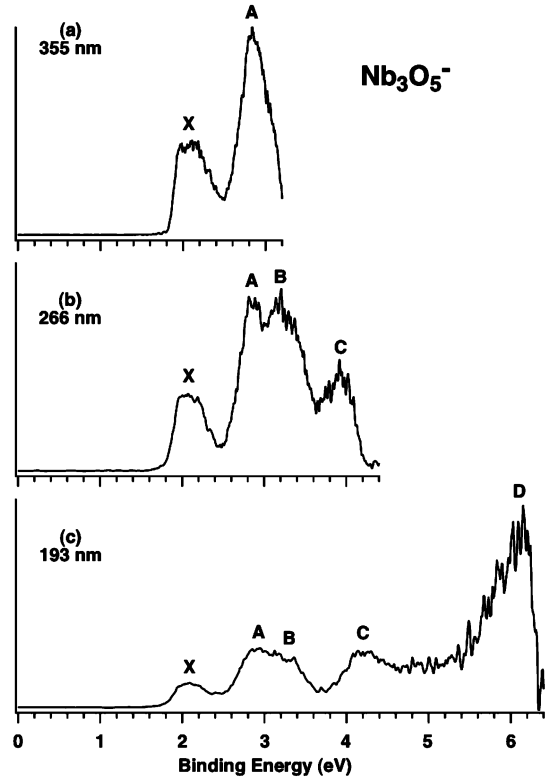

Figure 3. Photoelectron spectra of $Nb_3O_5^-$ at (a) 355, (b) 266, and (c) 193 nm.

3.3. $Nb_3O_5^-$. The PES spectra of $Nb_3O_5^-$ at three photon energies are shown in Figure 3. Four broad bands are observed below 4.5 eV: X (VDE: 2.09 eV), A (2.85 eV), B (∼3.2 eV), and C (∼4.2 eV). The electron affinity of Nb_3O_5 is evaluated to be 1.87 ± 0.03 eV from the reasonably well-defined onset of band X. A broad band D (centered at ∼6.1 eV) is observed at high binding energies, as shown in the 193 nm spectrum (Figure 3c).

3.4. $Nb_3O_6^-$. The PES spectra of $Nb_3O_6^-$ at two photon energies are shown in Figure 4. Two prominent bands are observed below 5 eV: X (VDE: 3.38 eV) and A (VDE: 4.57 eV). The higher binding energy side in the 193 nm spectrum (Figure 4b) is congested without any prominent features. A very weak feature X′ (VDE: 2.84 eV) is observed at low binding energies, which is likely due to a minor isomer. The X band represents the ground-state transition for the main isomer, yielding an electron affinity of 3.15 ± 0.05 eV for Nb_3O_6. The ADE for the minor isomer is estimated from band X′ to be ∼2.7 eV.

3.5. $Nb_3O_7^-$. The spectra of $Nb_3O_7^-$ at two photon energies are displayed in Figure 5, which are characterized by two prominent bands. The ground state X of $Nb_3O_7^-$ (ADE: 3.30 eV; VDE: 3.66 eV) is broad, followed by a large energy gap and an intense band A (Figure 5b). Band A occurs at such a high binding energy that its full width may not be accessed at 193 nm. The estimated ADE for band A is ∼5.9 eV, defining an X−A energy gap of ∼2.6 eV. Very weak signals X′ (ADE: ∼2.5 eV; VDE: ∼2.7 eV) are observed at the low binding energy side, likely due to a minor isomer.

3.6. $Nb_3O_8^-$. Because of its high electron binding energies, the PES spectrum of $Nb_3O_8^-$ is only measured at 193 nm, as shown in Figure 6. Only one broad band (labeled X) is revealed,

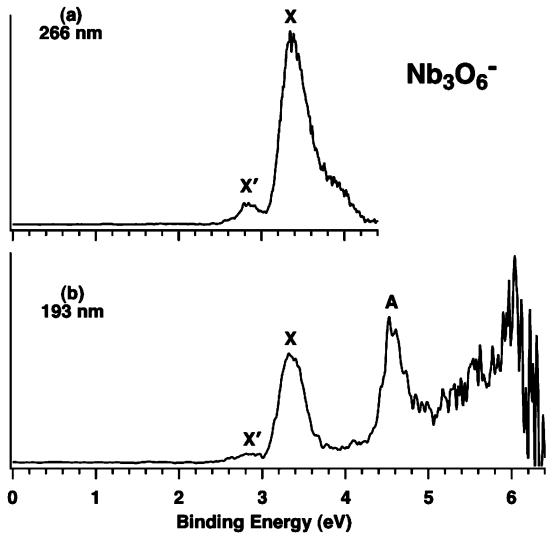

Figure 4. Photoelectron spectra of $Nb_3O_6^-$ at (a) 266 and (b) 193 nm. The weak X′ band represents a minor isomer.

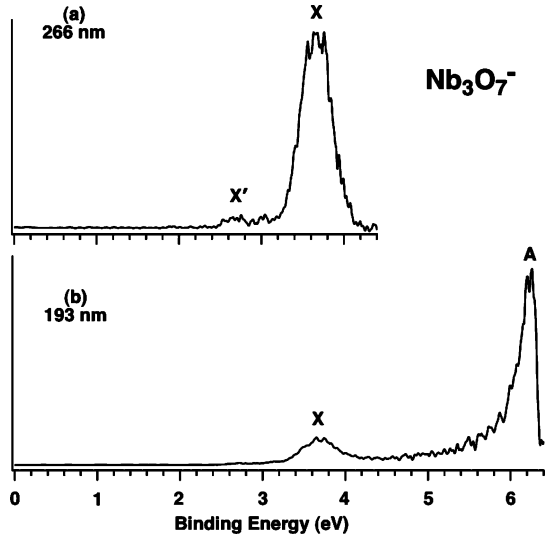

Figure 5. Photoelectron spectra of $Nb_3O_7^-$ at (a) 266 and (b) 193 nm. The weak X′ band represents a minor isomer.

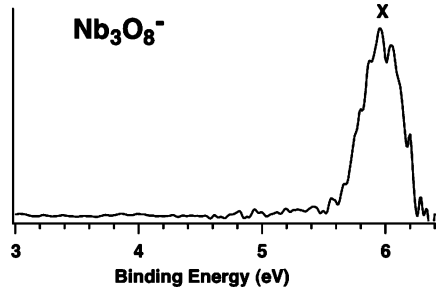

Figure 6. Photoelectron spectra of $Nb_3O_8^-$ at 193 nm. Note the high electron binding energies due to electron detachment from molecular orbitals of primarily O 2p characters.

which is centered at 5.97 eV. The electron affinity of Nb_3O_8 is evaluated to be 5.65 ± 0.05 eV from the reasonably well-defined band onset.

4. Theoretical Results

The optimized ground-state geometries and selected low-lying isomers of $Nb_3O_n^-$ and Nb_3O_n ($n = 3-8$) are presented in Figures 7 and 8, respectively, and their calculated VDEs are compared with the experimental values in Tables S1−S6 in the Supporting Information. The calculated relative energies at the B3LYP and BP86 levels for the lowest energy and selected low-lying isomers of $Nb_3O_n^-$ ($n = 3-8$) are shown in Table S7 in the Supporting Information. Only B3LYP results will be discussed in the text, unless stated otherwise. The simulated PES spectra from the lowest-energy anion structures and the selected low-lying isomers are shown in Figure 9. Alternative optimized structures are shown in the Supporting Information (Figures S1−S12), and all coordinates are given in the Supporting Information (Table S9). The calculated first VDEs from the low-lying anion cluster structures and their simulated PES spectra are compared with the experiment in the Supporting Information (Table S8 and Figures S13−S17).

4.1. $Nb_3O_3^-$ and Nb_3O_3. On the basis of our previous calculations on $Nb_3O_2^-$ and Nb_3O_2,[8] we performed an extensive search of the potential energy surfaces for $Nb_3O_3^-$ and Nb_3O_3, which appear to be rather flat with several closely lying isomers near the global minimum, as shown in Figures S1 and S2. The ground state of $Nb_3O_3^-$ is shown to be C_s ($^3A'$, Figure 7a), consisting of a triangular Nb_3 with one long Nb−Nb bond (2.956 Å) and two short Nb−Nb bonds (2.471 Å). The three O atoms are on bridging positions around the Nb_3 unit but are not in the same plane with one O atom above and two O atoms below the Nb_3 plane. A similar structure (C_s, $^3A'$) with two long Nb−Nb bonds (2.794 Å) and one short Nb−Nb bond (2.217 Å) is found to be only 0.04 eV higher in energy (Figure 7b). These two structures (Figures 7a,b), considered to be important in interpreting the experimental data, were reoptimized using the BP86 functional (Table S7). We found that the results at the BP86 level are very similar to those at B3LYP. Among other structures optimized for $Nb_3O_3^-$, the C_1 (^3A) and C_1 (^1A) structures with two bridging and one terminal oxygen are predicted to lie higher in energy than the ground state by 0.26 and 0.28 eV, respectively (Figures S1). Surprisingly, the ground state of the $Nb_3O_3^-$ cluster is substantially different from that of the valent isoelectronic $Ta_3O_3^-$ cluster, which was previously found to be D_{3h} ($^1A_1'$) with δ-aromaticity.[36,38]

For the neutral Nb_3O_3 cluster, we found a doublet state (C_s, $^2A''$, Figure 8a) to be the global minimum. Two similar structures with a doublet (C_s, $^2A'$) and a quartet (C_{2v}, $^4A_2$) spin multiplicity are found to be 0.16 and 0.27 eV above the ground state, respectively, as shown in Figure S2.

4.2. $Nb_3O_4^-$ and Nb_3O_4. Starting from the tribridged conformation of $Nb_3O_3^-$ and Nb_3O_3, we have considered different sites (terminal, bridging, and capping) to add the fourth O atoms in search of the ground states for $Nb_3O_4^-$ and Nb_3O_4 (Figures S3 and S4). The $Nb_3O_4^-$ and Nb_3O_4 ground states are predicted to be C_s ($^1A'$) (Figure 7c) and C_1 (^2A) (Figure 8b), respectively, with the fourth O atom occupying a terminal site. In both of the anionic and neutral ground states, the three bridging O atoms are above the plane of Nb_3, and the terminal O atom is below the Nb_3 plane. For $Nb_3O_4^-$, there are several low-lying isomers close to the ground state. The triplet structure (C_s, $^3A''$), very similar to the global minimum, is only 0.16 eV higher in energy (Figure S3). A second singlet state (C_s, $^1A'$) and two other triplet structures (C_1, ^3A and C_s, $^3A''$) are 0.18, 0.18, and 0.26 eV above the ground state, respectively (Figure S3). For the neutral, the second lowest doublet state (C_s, $^2A'$) with all four O atoms in the bridging positions is also fairly close to the ground state (C_1, ^2A) with a relative energy of 0.14 eV, as given in Figure S4.

4.3. $Nb_3O_5^-$ and Nb_3O_5. The potential energy surfaces for $Nb_3O_5^-$ and Nb_3O_5 are also rather flat with several closely lying

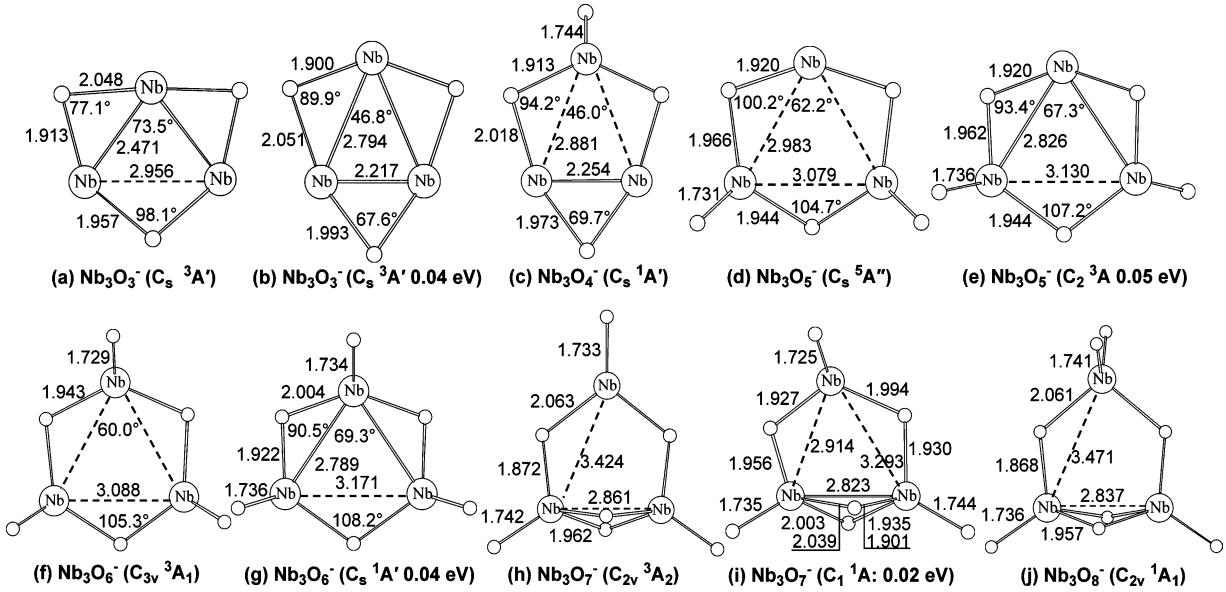

Figure 7. Optimized lowest-energy structures for $Nb_3O_n^-$ ($n = 3-8$) at the B3LYP level of theory. A closely lying isomer is presented for (b) $Nb_3O_3^-$, (e) $Nb_3O_5^-$, (g) $Nb_3O_6^-$, and (i) $Nb_3O_7^-$. Selected bond distances (angstroms) and bond angles (degrees) are shown.

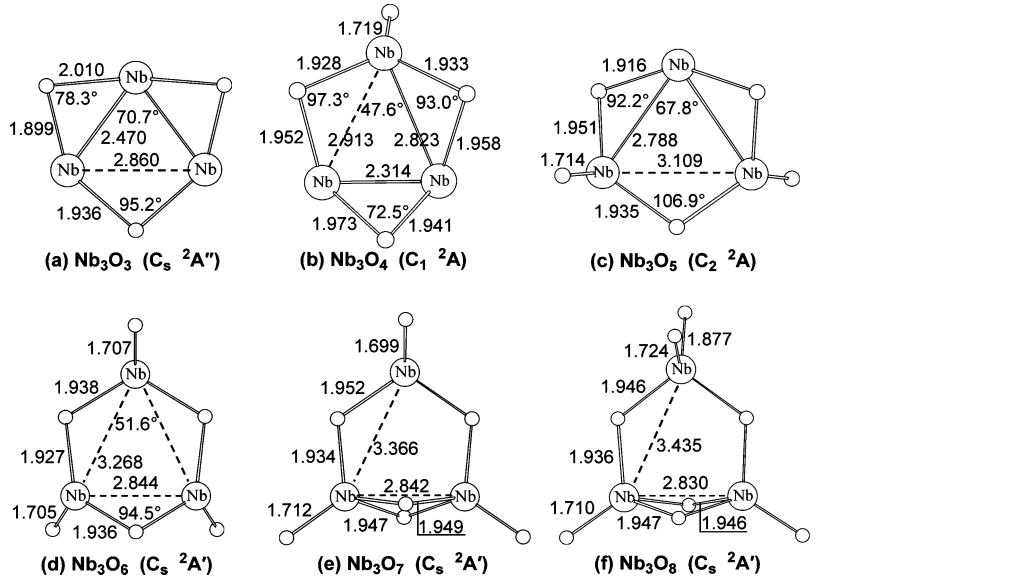

Figure 8. Ground-state structures for Nb_3O_n ($n = 3-8$) neutral clusters at the B3LYP level of theory. Selected bond distances (angstroms) and bond angles (degrees) are shown.

isomers near the global minimum (Figures S5 and S6). The lowest energy state of the $Nb_3O_5^-$ anion is predicted to be a high spin structure (C_s, $^5A''$) (Figure 7d), with the two low-spin states C_s ($^1A'$) and C_s ($^3A'$) being 0.34 and 0.22 eV higher in energy, respectively (Figure S5). A ^3A structure with C_2 symmetry for $Nb_3O_5^-$ is only 0.05 eV higher in energy (Figure 7e), essentially degenerate to the ground state. The singlet C_2 (^1A) state is 0.30 eV above the lowest energy state (Figure S5). Two other isomers with C_2 symmetry (^3B and ^5A) are 0.31 and 0.16 eV higher in energy (Figure S5), respectively. Overall, seven low-lying anion structures are located within 0.4 eV. These low-lying isomers are reoptimized at the BP86 level (Table S7). Interestingly, the triplet structure with C_2 symmetry at the B3LYP level (Figure 7e, 0.05 eV) becomes the ground state at the BP86 level. The ground state of the Nb_3O_5 neutral is found to be C_2 (^2A) (Figure 8c). All alternative neutral structures are at least 0.30 eV higher in energy (Figure S6).

4.4. $Nb_3O_6^-$ and Nb_3O_6. The ground state of the $Nb_3O_6^-$ anion is found to be a crown-shaped C_{3v} ($^3A_1$) (Figure 7f) at the B3LYP level with the bridging O atoms above and the three terminal O atoms below the Nb_3 plane. Its singlet state ($^1A'$) exhibits C_s symmetry, which is only 0.04 eV higher in energy (Figure 7g). At the BP86 level, the crown-shaped C_{3v} ($^3A_1$) structure is predicted to be slightly higher in energy than the singlet state (C_s, $^1A'$) by 0.10 eV (Table S7).

The neutral Nb_3O_6 ground state is found to be C_s ($^2A'$) (Figure 8d), differing from the anion mainly in the terminal oxygen directions with two terminal oxygen atoms pointed to one side and the third one pointed to the opposite side. Another C_s ($^2A'$) structure, similar to the anion ground state, is only 0.07 eV higher in energy (Figure S8). We also located two additional low-lying neutral isomers, both of which possess an O double-bridge and are only 0.09 and 0.28 eV higher in energy, respectively (Figure S8).

4.5. $Nb_3O_7^-$ and Nb_3O_7. A variety of structures were studied in search of the ground state of $Nb_3O_7^-$ and Nb_3O_7 (Figures S9 and S10). For the anion, the lowest-energy isomer is predicted to be an open-shell structure (C_{2v}, $^3A_2$) (Figure 7h). A closed-

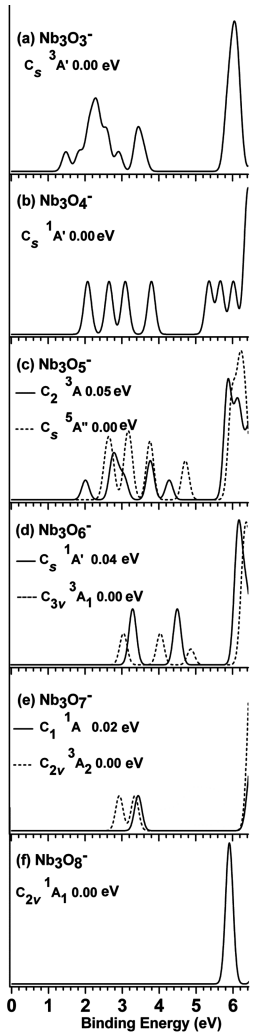

Figure 9. Simulated photoelectron spectra for the $Nb_3O_n^-$ ($n = 3-8$) clusters from the lowest-energy and selected low-lying structures. The simulations are done by fitting the distribution of calculated VDEs with unit-area Gaussian functions of 0.1 eV width.

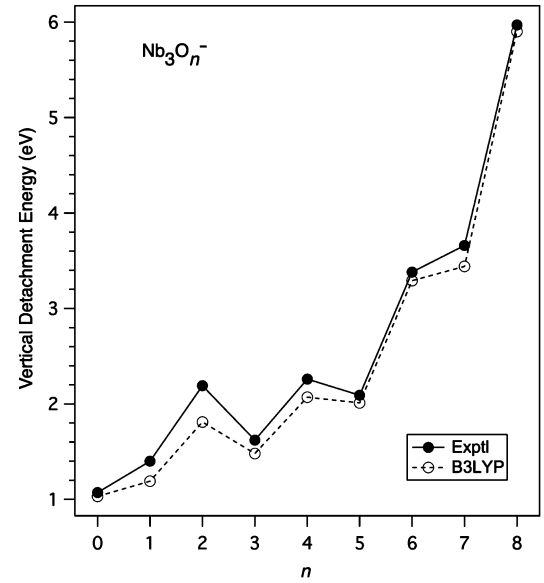

Figure 10. Experimental (solid line) and theoretical (dashed line) ground-state vertical detachment energies for $Nb_3O_n^-$ ($n = 0-8$) as a function of O content. Vertical detachment energies for Nb_3^-, Nb_3O^-, and $Nb_3O_2^-$ are taken from ref 8 .

shell, lower symmetry structure (C_1, ^{1}A) (Figure 7i) is only 0.02 eV above the lowest energy structure, and the corresponding triplet state (C_1, ^{3}A) is 0.16 eV higher in energy (Figure S9). A (C_s, ^{1}A′) structure with a capping O atom is found to be 0.14 eV higher than the ground state (Figure S9). At the BP86 level, the closed-shell (C_1, ^{1}A) structure becomes the ground state (Table S7). The ground state of Nb_3O_7 favors a doublet with C_s (^{2}A′) symmetry, as shown in Figure 8e. All other optimized isomers of the neutral cluster are significantly higher (>0.4 eV) in energy, as shown in Figure S10.

4.6. $Nb_3O_8^-$ and Nb_3O_8. The ground state of anionic $Nb_3O_8^-$ is a singlet C_{2v} (^{1}A$_1$) structure (Figure 7j) with four bridging and four terminal O atoms. An anion isomer C_{2v} (^{1}A$_1$) with five bridging oxygens and three terminal oxygens is 0.41 eV above the ground state (Figure S11). The ground state of Nb_3O_8 is ^{2}A′ with C_s symmetry (Figure 8f). A C_s (^{2}A″) structure is located 0.38 eV above the ground state (Figure S12). Structures with a capping O atom are found substantially higher in energy for all $Nb_3O_8^-$ and Nb_3O_8 species (Figures S11 and S12).

5. Discussion

5.1. Comparison between Experiment and Theory. The resolved PES bands in Figures 1−6 serve as electronic fingerprint for the $Nb_3O_n^-$ ($n = 3-8$) clusters, allowing comparisons with theoretical calculations to verify the identified global minimum structures.[54] The calculated ground-state VDEs are compared with the experimental values in Table 1, whereas their simulated PES spectra are shown in Figure 9. As seen in Table 1, B3LYP underestimates the ground-state VDEs for $Nb_3O_n^-$, with typical discrepancies ranging from ∼0.1 eV (for $Nb_3O_3^-$, $Nb_3O_5^-$, $Nb_3O_6^-$, and $Nb_3O_8^-$) to ∼0.2 eV (for $Nb_3O_4^-$ and $Nb_3O_7^-$). However, the general VDE trend for $Nb_3O_n^-$ versus O content is in excellent agreement with the experimental data, as shown in Figure 10, lending considerable credence to the identified anion cluster structures. The overall simulated PES patterns (Figure 9) are also in reasonable agreement with the experimental spectra for all $Nb_3O_n^-$ ($n = 3-8$) clusters, especially for the $Nb_3O_4^-$ and $Nb_3O_8^-$ clusters. The four low binding energy bands of $Nb_3O_4^-$ (Figure 2) and the single band in $Nb_3O_8^-$ agree very well with the experimental spectra, leaving little doubt about the global minimum structures predicted computationally. Therefore, in the following, we will mainly focus our discussion on $Nb_3O_3^-$, $Nb_3O_5^-$, $Nb_3O_6^-$, and $Nb_3O_7^-$.

For $Nb_3O_3^-$, the simulated PES patterns on the basis of the two nearly degenerate triplet C_s (^{3}A′) isomers (Figure 7a,b) appear to be rather similar, both being extremely congested and consisting of some 10 electronic states within the 1.4−3.8 eV regime (Table S1, Supporting Information). Experimentally, we were able to resolve nine electronic transitions within the same binding energy range (Figure 1). Close comparisons of the VDE patterns (Table S1) allow us to conclude that the lowest energy C_s (^{3}A′) isomer (Figure 7a), which can qualitatively generate all observed electronic transitions except for E or F, is probably the major carrier for the observed spectra, although we cannot rule out minor contributions from the low-lying isomer shown in Figure 7b. The predicted first VDE (1.48 eV) for the global minimum structure is slightly lower than the experiment (1.62 eV), consistent with the general trend of the B3LYP performance (Figure 10).

The B3LYP calculations favor a quintet state C_s (^{5}A″) (Figure 7d) for $Nb_3O_5^-$, but the simulated PES pattern for the lowest triplet state C_2 (^{3}A) (Figure 7e) appears to be in better agreement with the experiment, reproducing all prominent PES bands (X, A, B, C, and D; Figure 9c). However, the broad and continuous

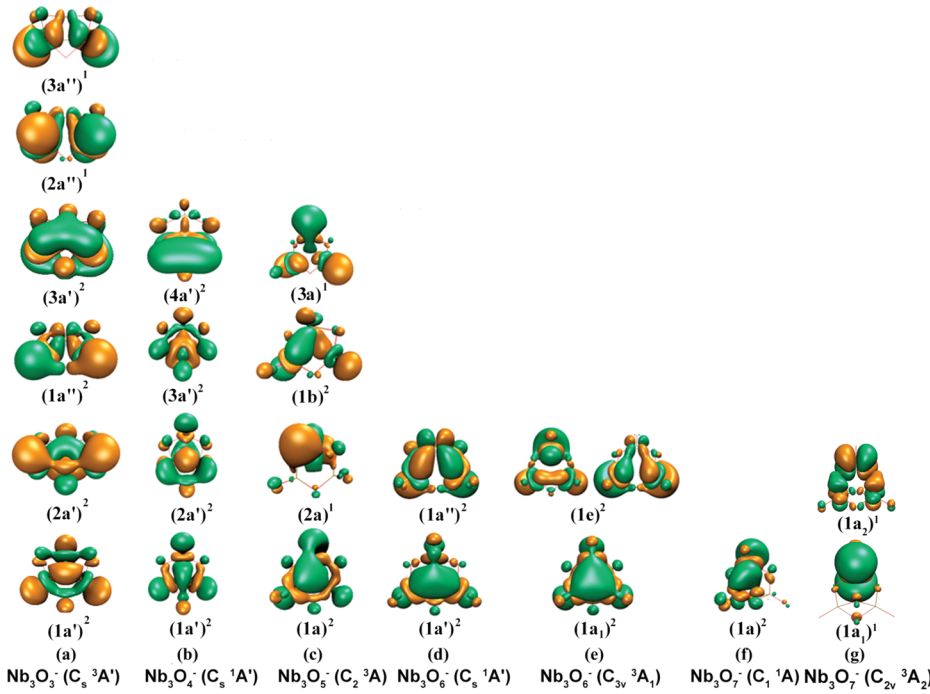

Figure 11. Pictures of the Nb-derived valence molecular orbitals for $Nb_3O_n^-$ ($n = 3-7$).

PES pattern (Figure 3) suggests the possibility of the quintet state C_s ($^5A''$) being populated in the $Nb_3O_5^-$ cluster beam as a minor isomer.

For $Nb_3O_6^-$, the second lowest isomer C_s ($^1A'$) (Figure 7g), which is only 0.04 eV above the triplet C_{3v} ($^3A_1$) structure (Figure 7f) at the B3LYP level, is in excellent agreement with the experiment, reproducing well the prominent PES bands (X and A; Figure 9d) and suggesting that the C_s ($^1A'$) structure should be the global minimum for $Nb_3O_6^-$. The simulated spectrum for the C_{3v} ($^3A_1$) structure displays a low binding energy feature and should be attributed to the weak X′ feature observed experimentally, implying that the C_{3v} structure is a low-lying isomer.

For $Nb_3O_7^-$, the B3LYP calculations slightly favor a triplet state C_{2v} ($^3A_2$) (Figure 7h). Its simulated spectrum displays a low binding energy feature (Figure 9e), which should be assigned to the weak X′ feature (Figure 5a) observed experimentally. As shown in Table 1, Figure 9e, and Table S5, the calculated VDEs and the simulated PES spectrum for the singlet state (C_1, ^1A) (Figure 7i) are in good agreement with the experimental data, and it should be the dominant species observed. Therefore, the ground state of $Nb_3O_7^-$ should be the singlet structure (Figure 7i) with the triplet state (Figure 7h) as a low-lying isomer.

Additional simulations for low-lying $Nb_3O_n^-$ ($n = 3-8$) isomers (within ~0.4 eV) are shown in the Supporting Information (Figures S13−S17), which are in worse agreement with the experimental data. The comparison of the theoretical and experimental data provides considerable credence for the global minimum and low-lying isomers obtained for the $Nb_3O_n^-$ ($n = 3-8$) clusters from the DFT calculations. For the $Nb_3O_6^-$ and $Nb_3O_7^-$ clusters, definitive experimental evidence is observed for two isomers, as borne out from the calculations. It is likely that the spectra of $Nb_3O_3^-$ and $Nb_3O_5^-$ also contain contributions from minor isomers.

5.2. Structural Evolution and Sequential Oxidation of $Nb_3O_n^-$ ($n = 3-8$). Starting from the C_s structure $Nb_3O_3^-$, in which all three O atoms occupy the bridging sites, the next three O atoms in $Nb_3O_n^-$ ($n = 4-6$) successively occupy the terminal sites. The seventh O atom in the $Nb_3O_7^-$ cluster is again bridge-bonded to the cyclic structure of $Nb_3O_6^-$, forming a double-bridge. The $Nb_3O_8^-$ cluster is formed from $Nb_3O_7^-$ with the extra O atom bonded to a terminal site, in which each Nb atom has reached to its maximum oxidation state of +5. The ground-state structures of $Nb_3O_n^-$ and Nb_3O_n ($n = 3-8$) are all nonplanar with low symmetries, consistent with their broad PES features, which are also borne out from the large geometry changes from the anions to the neutrals. A previous theoretical study of the $Nb_mO_n^{0/+}$ ($m = 1-3$; $n = 2-5$, 7, 8) clusters suggested that Nb_3O_7 and Nb_3O_8 possess chain-type structures,[29] which are in fact much higher in energy.

Figure 10 compares the experimental and calculated VDEs for the entire $Nb_3O_n^-$ series from $n = 0-8$. The VDE trend as a function of O content in $Nb_3O_n^-$ is similar to that for the valent isoelectronic $Ta_3O_n^-$ clusters.[36] Significant differences in the VDE trend are found from other metal oxide clusters, such as in $Fe_mO_n^-$, $Cu_2O_n^-$, $Al_3O_n^-$, and $V_2O_n^-$,[55] which display nearly linear increases as a function of n. The VDE trend in $Nb_3O_n^-$ ($n = 0-8$) seems to exhibit a zigzag pattern (Figure 10), which is related to the spin states of the clusters. Both $Nb_3O_2^-$ and $Nb_3O_4^-$ are closed shell, and thus they have higher VDEs than the open shell $Nb_3O_3^-$ and $Nb_3O_5^-$, respectively. Niobium has an electron configuration of $4d^45s^1$. With the increase in the number of O atoms, the 16 valence electrons of Nb_3^- can be viewed to be sequentially transferred to the O atom with increasing n, until all valence electrons of Nb_3^- are transferred to the O atoms in $Nb_3O_8^-$, in which each Nb atom has reached the maximum oxidation state of +5.

The overall VDE trend can be qualitatively understood from the MO analysis shown in Figure 11, and it is related to the nature of the HOMO. The HOMOs from $n = 3-5$ are either antibonding or nonbonding, leading to their relatively low VDEs. The HOMOs of $n = 6$ and 7 involve either a partially Nb−Nb bonding orbital ($n = 6$) or a localized orbital ($n = 7$), consistent with their significantly increased VDEs. Detachment features for the Nb s/d-based MOs always occur at lower binding

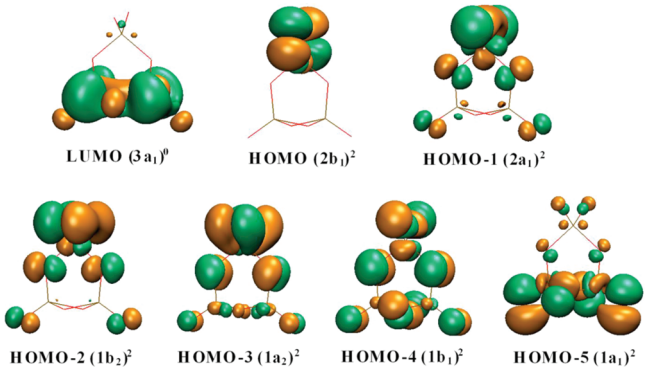

Figure 12. Frontier molecular orbital pictures for $Nb_3O_8^-$.

energies, whereas those from O 2p are at much higher binding energies, usually beyond 5 eV. Therefore, the extremely high VDE of $Nb_3O_8^-$, which formally possesses all Nb(5+) centers, is due to electron detachment from O 2p-type MOs, as shown in Figure 12. This series of multinuclear clusters may be viewed as molecular models for mechanistic understandings of the oxidation of Nb surfaces.[56]

5.3. Comparison with Analogous Clusters: $Nb_3O_n^-$ versus $Ta_3O_n^-$. We have previously reported a similar study on the valent-isoelectronic trinuclear tantalum oxide clusters, $Ta_3O_n^-$ ($n = 0-8$).[36] The overall electronic evolution and sequential oxidation of the two systems as a function of O content appear rather similar, consistent with their similar structural evolutions. Specifically, the ground-state VDEs of $Nb_3O_n^-$ and $Ta_3O_n^-$ are very similar within 0.1 to 0.3 eV, with the Ta clusters normally possessing slightly higher VDE values. However, there are two notable exceptions. First, the VDE for $Nb_3O_2^-$ (2.19 eV) is substantially greater than that of $Ta_3O_2^-$ (1.675 eV) by ~0.5 eV. This can be attributed to the unusual C_1 (^{1}A) ground-state structure of $Nb_3O_2^-$ with a terminal O atom and readily rationalized on the basis of MO analysis.[8] Indeed, our DFT calculations showed that the dibridged structure, which is similar to the global minimum of $Ta_3O_2^-$ but is a higher energy isomer for $Nb_3O_2^-$, should possess a much lower VDE (1.33 eV).[8] Second, the VDE for $Nb_3O_3^-$ (1.62 eV) is smaller than that of $Ta_3O_3^-$ (2.253 eV) by as much as ~0.6 eV. The $Ta_3O_3^-$ cluster is characterized as a δ-aromatic molecule with a perfect D_{3h} (^{1}A$_1'$) planar triangular structure.[38] However, the corresponding D_{3h} singlet state for $Nb_3O_3^-$ does not exist. Conversely, an open-shell, nonplanar C_s (^{3}A′) structure with one long bond and two short bonds is located as the ground state for $Nb_3O_3^-$ (Figure 7a). The PES patterns of $Nb_3O_3^-$ and $Ta_3O_3^-$ are also quite different, reflecting their different electronic ground states. The difference in $Nb_3O_3^-$ versus $Ta_3O_3^-$ may be traced to the δ aromaticity in the latter, which leads to enhanced electronic stabilization to $Ta_3O_3^-$, as reflected from its significantly higher first VDE relative to $Nb_3O_3^-$.

In terms of electronic spin states, the $Nb_3O_n^-$ and $Ta_3O_n^-$ clusters also show some differences. For the Ta clusters, all $n = 1-8$ species are shown to be dominated by closed-shell structures, with triplet structures coexisting in the molecular beam as a minor isomer only for the $Ta_3O_5^-$ and $Ta_3O_6^-$ clusters.[36] However, for the Nb clusters, only $Nb_3O_2^-$, $Nb_3O_4^-$, and $Nb_3O_8^-$ possess singlet ground states, whereas all $Nb_3O_n^-$ ($n = 3$, 5, 6, and 7) clusters are observed to possess triplet states as either dominant species ($Nb_3O_3^-$ and $Nb_3O_5^-$) or as a minor isomer ($Nb_3O_6^-$ and $Nb_3O_7^-$). Indeed, even the quintet spin states are fairly low-lying isomers for $Nb_3O_5^-$ (Table 1). Therefore, there appears to be a clear tendency for the Nb oxide clusters to adopt high spin structures rather than closed-shell states. These differences in the structure and bonding between the Nb and Ta clusters are due to weaker metal−metal bonding in the 4d Nb systems relative to that in the 5d Ta systems, which should have interesting implications in the chemical and catalytic properties in Nb and Ta oxides materials.

6. Conclusions

PES has been combined with DFT calculations to study the electronic and structural evolution as a function of composition for the triniobium oxide clusters, $Nb_3O_n^-$ ($n = 3-8$). PES spectra are obtained for the anion clusters at various photon energies, allowing the detachment from both the Nb 6s/5d-based electronic states and the O 2p states. Extensive DFT calculations are performed at the B3LYP level in search of the lowest energy structures for both the anions and neutrals. Simulated PES spectra for the global minimum and low-lying isomers are compared with the experimental PES data. For $Nb_3O_3^-$, all three O atoms are shown to prefer the bridging sites of the triangular Nb_3. The next three O atoms in $Nb_3O_n^-$ ($n = 4-6$) successively occupy the three terminal sites. The seventh and eighth O atoms are shown to form a double-bridge and a double-terminal, respectively, reaching the stoichiometric $Nb_3O_8^-$, in which each Nb atom achieves the maximum oxidation state of +5. The global minima of the $Nb_3O_n^-$ ($n = 3-8$) clusters are all nonplanar with multiple low-lying isomers for several systems. The $Nb_3O_4^-$ and $Nb_3O_8^-$ clusters possess singlet ground states, whereas the $Nb_3O_n^-$ ($n = 3$, 5, 6, and 7) clusters all exhibit high spin states. In comparison with the $Ta_3O_n^-$ series, the high-spin states and low-symmetry structures of the $Nb_3O_n^-$ clusters can be attributed to the weaker d−d bonding by Nb, which may give rise to higher reactivities and catalytic activities to the niobium oxide systems.

Acknowledgment. The experimental work was supported by the Chemical Sciences, Geosciences and Biosciences Division, Office of Basic Energy Sciences, U.S. Department of Energy (DOE) under grant no. DE-FG02-03ER15481 (catalysis center program). X.H. gratefully acknowledges supports from the Natural Science Foundation of China (20771026 and 90922022) and the Natural Science Foundation of Fujian Province of China (no. 2008J0151).

Supporting Information Available: Comparisons of experimental and calculated electron detachment energies, the calculated relative energies at the B3LYP and BP86 levels for the lowest energy and selected low-lying isomers of $Nb_3O_n^-$ ($n = 3-8$), the calculated first VDEs from the low-lying anion cluster structures compared with the experiment, alternative optimized anion and neutral cluster structures and their Cartesian coordinates, and simulated PES spectra from low-lying anion structures. This material is available free of charge via the Internet at http://pubs.acs.org.

References and Notes

(1) Nowak, I.; Ziolek, M. *Chem. Rev.* **1999**, *99*, 3603.
(2) Ziolek, M. *Catal. Today* **2003**, *78*, 47.
(3) Tanabe, K. *Catal. Today* **2003**, *78*, 65.
(4) Wachs, I. E.; Chen, Y. S.; Jehng, J. M.; Briand, L. E.; Tanaka, T. *Catal. Today* **2003**, *78*, 13.
(5) Ohuchi, T.; Miyatake, T.; Hitomi, Y.; Tanaka, T. *Catal. Today* **2007**, *120*, 233.
(6) Oliver, J. M.; Nieto, J.M. L.; Botella, P. *Catal. Today* **2004**, *96*, 241.
(7) Böhme, D. K.; Schwarz, H. *Angew. Chem., Int. Ed.* **2005**, *44*, 2336.
(8) Zhai, H. J.; Wang, B.; Huang, X.; Wang, L. S. *J. Phys. Chem. A* **2009**, *113*, 3866.

(9) (a) Morse, M. D. *Chem. Rev.* **1986**, *86*, 1049. (b) Loh, S. K.; Lian, L.; Armentrout, P. B. *J. Am. Chem. Soc.* **1989**, *111*, 3167. (c) Knickelbein, M. B.; Yang, S. H. *J. Chem. Phys.* **1990**, *93*, 5760.

(10) (a) Wang, H. M.; Craig, R.; Haouari, H.; Liu, Y. F.; Lombardi, J. R.; Lindsay, D. M. *J. Chem. Phys.* **1996**, *105*, 5355. (b) Aydin, M.; Lombardi, J. R. *Int. J. Mass Spectrom.* **2004**, *235*, 91.

(11) Song, L.; Eychmuller, A.; St. Pierre, R. J.; El-Sayed, M. A. *J. Phys. Chem.* **1989**, *93*, 2485.

(12) Athanassenas, K.; Kreisle, D.; Collings, B. A.; Rayner, D. M.; Hackett, P. A. *Chem. Phys. Lett.* **1993**, *213*, 105.

(13) Kietzmann, H.; Morenzin, J.; Bechthold, P. S.; Gantefor, G.; Eberhardt, W.; Yang, D. S.; Hackett, P. A.; Fournier, R.; Pang, T.; Chen, C. F. *Phys. Rev. Lett.* **1996**, *77*, 4528.

(14) Kietzmann, H.; Morenzin, J.; Bechthold, P. S.; Gantefor, G.; Eberhardt, W. *J. Chem. Phys.* **1998**, *109*, 2275.

(15) Deng, H. T.; Kerns, K. P.; Castleman, A. W., Jr. *J. Phys. Chem.* **1996**, *100*, 13386.

(16) (a) Zemski, K. A.; Justes, D. R.; Bell, R. C.; Castleman, A. W., Jr. *J. Phys. Chem. A* **2001**, *105*, 4410. (b) Zemski, K. A.; Justes, D. R.; Castleman, A. W., Jr. *J. Phys. Chem. A* **2001**, *105*, 10237. (c) Zemski, K. A.; Justes, D. R.; Castleman, A. W., Jr. *J. Phys. Chem. B* **2002**, *106*, 6136. (d) Justes, D. R.; Moore, N. A.; Castleman, A. W., Jr. *J. Phys. Chem. B* **2004**, *108*, 3855.

(17) Green, S. M. E.; Alex, S.; Fleischer, N. L.; Millam, E. L.; Marcy, T. P.; Leopold, D. G. *J. Chem. Phys.* **2001**, *114*, 2653.

(18) (a) Fielicke, A.; Meijer, G.; von Helden, G. *J. Am. Chem. Soc.* **2003**, *125*, 3659. (b) Fielicke, A.; Meijer, G.; von Helden, G. *J. Chem. Phys.* **2007**, *127*, 234306.

(19) Molek, K. S.; Jaeger, T. D.; Duncan, M. A. *J. Chem. Phys.* **2005**, *123*, 144313.

(20) Dong, F.; Heinbuch, S.; He, S. G.; Xie, Y.; Rocca, J. J.; Bernstein, E. R. *J. Chem. Phys.* **2006**, *125*, 164318.

(21) Sigsworth, S. W.; Castleman, A. W., Jr. *J. Am. Chem. Soc.* **1992**, *114*, 10471.

(22) Yang, D. S.; Zgierski, M. Z.; Rayner, D. M.; Hackett, P. A.; Martinez, A.; Salahub, D. R.; Roy, P. N.; Carrington, T., Jr. *J. Chem. Phys.* **1995**, *103*, 5335.

(23) (a) Jackson, P.; Fisher, K. J.; Willett, G. D. *Int. J. Mass Spectrom.* **2000**, *197*, 95. (b) Jackson, P.; Fisher, K. J.; Willett, G. D. *Chem. Phys.* **2000**, *262*, 179.

(24) Dryza, V.; Addicoat, M. A.; Gascooke, J. R.; Buntine, M. A.; Metha, G. F. *J. Phys. Chem. A* **2008**, *112*, 5582.

(25) Sellers, H. *J. Phys. Chem.* **1990**, *94*, 1338.

(26) Goodwin, L.; Salahub, D. R. *Phys. Rev. A* **1993**, *47*, R774.

(27) Grönbeck, H.; Rosén, A. *Phys. Rev. B* **1996**, *54*, 1549.

(28) Fournier, R.; Pang, T.; Chen, C. F. *Phys. Rev. A* **1998**, *57*, 3683.

(29) Sambrano, J. R.; Andres, J.; Beltran, A.; Sensato, F.; Longo, E. *Chem. Phys. Lett.* **1998**, *287*, 620.

(30) Fowler, J. E.; García, A.; Ugalde, J. M. *Phys. Rev. A* **1999**, *60*, 3058.

(31) (a) Majumdar, D.; Balasubramanian, K. *J. Chem. Phys.* **2001**, *115*, 885. (b) Majumdar, D.; Balasubramanian, K. *J. Chem. Phys.* **2003**, *119*, 12866.

(32) Balasubramanian, K.; Zhu, X. L. *J. Chem. Phys.* **2001**, *114*, 10375.

(33) Martinez, A.; Calaminici, P.; Koster, A. M.; Salahub, D. R. *J. Chem. Phys.* **2001**, *114*, 819.

(34) Calaminici, P.; Flores-Moreno, R.; Koster, A. M. *J. Chem. Phys.* **2004**, *121*, 3558.

(35) Addicoat, M. A.; Buntine, M. A.; Yates, B.; Metha, G. F. *J. Comput. Chem.* **2008**, *29*, 1497.

(36) (a) Zhai, H. J.; Wang, B.; Huang, X.; Wang, L. S. *J. Phys. Chem. A* **2009**, *113*, 9804. (b) Wang, B.; Zhai, H. J.; Huang, X.; Wang, L. S. *J. Phys. Chem. A* **2008**, *112*, 10962.

(37) (a) Zhai, H. J.; Kiran, B.; Cui, L. F.; Li, X.; Dixon, D. A.; Wang, L. S. *J. Am. Chem. Soc.* **2004**, *126*, 16134. (b) Huang, X.; Zhai, H. J.; Waters, T.; Li, J.; Wang, L. S. *Angew. Chem., Int. Ed.* **2006**, *45*, 657. (c) Zhai, H. J.; Wang, L. S. *J. Am. Chem. Soc.* **2007**, *129*, 3022. (d) Zhai, H. J.; Döbler, J.; Sauer, J.; Wang, L.-S. *J. Am. Chem. Soc.* **2007**, *129*, 13270. (e) Zhai, H. J.; Li, S. G.; Dixon, D. A.; Wang, L. S. *J. Am. Chem. Soc.* **2008**, *130*, 5167.

(38) Zhai, H. J.; Averkiev, B. B.; Zubarev, D. Yu.; Wang, L. S.; Boldyrev, A. I. *Angew. Chem., Int. Ed.* **2007**, *46*, 4277.

(39) (a) Huang, X.; Zhai, H. J.; Kiran, B.; Wang, L. S. *Angew. Chem., Int. Ed.* **2005**, *44*, 7251. (b) Zubarev, D. Yu.; Averkiev, B. B.; Zhai, H. J.; Wang, L. S.; Boldyrev, A. I. *Phys. Chem. Chem. Phys.* **2008**, *10*, 257.

(40) (a) Wang, L. S.; Cheng, H. S.; Fan, J. *J. Chem. Phys.* **1995**, *102*, 9480. (b) Wang, L. S.; Wu, H. In *Advances in Metal and Semiconductor Clusters: Cluster Materials*; Duncan, M. A., Ed.; JAI Press: Greenwich, CT, 1998; Vol. 4, pp 299−343.

(41) (a) Wang, L. S.; Li, X. In *Clusters and Nanostructure Interfaces*; Jena, P., Khanna, S. N., Rao, B. K., Eds.; World Scientific: NJ, 2000; pp 293−300. (b) Akola, J.; Manninen, M.; Hakkinen, H.; Landman, U.; Li, X.; Wang, L. S. *Phys. Rev. B* **1999**, *60*, R11297. (c) Wang, L. S.; Li, X.; Zhang, H. F. *Chem. Phys.* **2000**, *262*, 53. (d) Zhai, H. J.; Wang, L. S.; Alexandrova, A. N.; Boldyrev, A. I. *J. Chem. Phys.* **2002**, *117*, 7917.

(42) Becke, A. D. *J. Chem. Phys.* **1993**, *98*, 1372.

(43) Lee, C.; Yang, W.; Parr, R. G. *Phys. Rev. B* **1988**, *37*, 785.

(44) Stephens, P. J.; Devlin, F. J.; Chabalowski, C. F.; Frisch, M. J. *J. Phys. Chem.* **1994**, *98*, 11623.

(45) Andrae, D.; Haeussermann, U.; Dolg, M.; Stoll, H.; Preuss, H. *Theor. Chim. Acta* **1990**, *77*, 123.

(46) Küchle, W.; Dolg, M.; Stoll, H.; Preuss, H. Pseudopotentials of the Stuttgart/Dresden Group 1998, revision August 11, 1998. http://www.theochem.uni-stuttgart.de/pseudopotentials.

(47) Martin, J. M. L.; Sundermann, A. *J. Chem. Phys.* **2001**, *114*, 3408.

(48) Dunning, T. H., Jr. *J. Chem. Phys.* **1989**, *90*, 1007.

(49) Kendall, R. A.; Dunning, T. H., Jr.; Harrison, R. J. *J. Chem. Phys.* **1992**, *96*, 6796.

(50) Perdew, J. P. *Phys. Rev. B* **1986**, *33*, 8822.

(51) Tozer, D. J.; Handy, N. C. *J. Chem. Phys.* **1998**, *109*, 10180.

(52) Frisch, M. J.; Trucks, G. W.; Schlegel, H. B.; Scuseria, G. E.; Robb, M. A.; Cheeseman, J. R.; Montgomery, J. A., Jr.; Vreven, T.; Kudin, K. N.; Burant, J. C.; Millam, J. M.; Iyengar, S. S.; Tomasi, J.; Barone, V.; Mennucci, B.; Cossi, M.; Scalmani, G.; Rega, N.; Petersson, G. A.; Nakatsuji, H.; Hada, M.; Ehara, M.; Toyota, K.; Fukuda, R.; Hasegawa, J.; Ishida, M.; Nakajima, T.; Honda, Y.; Kitao, O.; Nakai, H.; Klene, M.; Li, X.; Knox, J. E.; Hratchian, H. P.; Cross, J. B.; Bakken, V.; Adamo, C.; Jaramillo, J.; Gomperts, R.; Stratmann, R. E.; Yazyev, O.; Austin, A. J.; Cammi, R.; Pomelli, C.; Ochterski, J. W.; Ayala, P. Y.; Morokuma, K.; Voth, G. A.; Salvador, P.; Dannenberg, J. J.; Zakrzewski, V. G.; Dapprich, S.; Daniels, A. D.; Strain, M. C.; Farkas, O.; Malick, D. K.; Rabuck, A. D.; Raghavachari, K.; Foresman, J. B.; Ortiz, J. V.; Cui, Q.; Baboul, A. G.; Clifford, S.; Cioslowski, J.; Stefanov, B. B.; Liu, G.; Liashenko, A.; Piskorz, P.; Komaromi, I.; Martin, R. L.; Fox, D. J.; Keith, T.; Al-Laham, M. A.; Peng, C. Y.; Nanayakkara, A.; Challacombe, M.; Gill, P. M. W.; Johnson, B.; Chen, W.; Wong, M. W.; Gonzalez, C.; Pople, J. A. *Gaussian03*, revision D. 01; Gaussian, Inc.: Wallingford, CT, 2004.

(53) VMD (Visual Molecular Dynamics): Humphrey, W.; Dalke, A.; Schulten, K. *J. Mol. Graphics* **1996**, *14*, 33.

(54) We have recently shown in a combined experimental and theoretical study that the B3LYP level of theory performs very well for the $Nb_3O_2^-$ cluster (ref 5). The current calculations on $Nb_3O_n^{-/0}$ ($n = 3-8$) were done using the same method and basis sets.

(55) (a) Wang, L. S.; Wu, H.; Desai, S. R. *Phys. Rev. Lett.* **1996**, *76*, 4853. (b) Wang, L. S.; Wu, H.; Desai, S. R.; Lou, L. *Phys. Rev. B* **1996**, *53*, 8028. (c) Wu, H.; Li, X.; Wang, X. B.; Ding, C. F.; Wang, L. S. *J. Chem. Phys.* **1998**, *109*, 449. (d) Zhai, H. J.; Wang, L. S. *J. Chem. Phys.* **2002**, *117*, 7882.

(56) (a) Franchy, R.; Bartke, T. U.; Gassmann, P. *Surf. Sci.* **1996**, *366*, 60. (b) An, B.; Fukuyama, S.; Yokogawa, K.; Yoshimura, M. *Phys. Rev. B* **2003**, *68*, 115423. (c) Arfaoui, I.; Cousty, J.; Guillot, C. *Surf. Sci.* **2004**, *557*, 119. (d) Kilimis, D. A.; Lekka, Ch. E. *Mater. Sci. Eng., B* **2007**, *144*, 27.

JP102439V